Title: Channel catfish use higher coordination to capture prey than to swallow

Short title: A shift in coordination during feeding

Journal: Proceedings of the Royal Society B

Article type: Research

Authors: Aaron M. Olsen[1], L. Patricia Hernández[2], Ariel L. Camp[1,3], Elizabeth L. Brainerd[1]

Author affiliations: [1]Brown University, [2]The George Washington University, [3]University of Liverpool

Keywords: biomechanics, animal motion, motion integration, motor control, XROMM

Words: 7,000

When animals move they must coordinate motion among multiple parts of the musculoskeletal system. Different behaviors exhibit different patterns of coordination, however it remains unclear what general principles determine the coordination pattern for a particular behavior. One hypothesis is that speed determines coordination patterns as a result of differences in voluntary versus involuntary control. An alternative hypothesis is that the nature of the behavioral task determines patterns of coordination. Suction-feeding fishes have highly kinetic skulls and must coordinate the motions of over a dozen skeletal elements to draw fluid and prey into the mouth. We used a dataset of intracranial motions at 5 cranial joints in channel catfish (*Ictalurus punctatus*), collected using X-ray reconstruction of moving morphology, to test whether speed or task best explained patterns of coordination. We found that motions were significantly more coordinated (by 20-29%) during prey capture than during prey transport, supporting the hypothesis that the nature of the task determines coordination patterns. We found no significant difference in coordination between low- versus high-speed motions. We speculate that capture is more coordinated to create a single fluid flow into the mouth while transport is less coordinated so that the cranial elements can independently generate multiple flows to reposition prey. Our results demonstrate the benefits of both higher and lower coordination in animal behaviors and the potential of motion analysis to elucidate motor tasks.

1. Introduction

Central to the diversity of animal movements, including those of humans, is the coordinated motion of multiple components of the musculoskeletal system. In its colloquial use 'coordinated' may describe someone who is adept at a particular task or sport. However, in its technical sense 'coordination' refers to the strength of correlated motion among different body parts due to active, neural processes [1,2], typically measured using cross-correlation or continuous relative phase [3]. Since environmental interactions are often unpredictable, the neural system cannot coordinate motion simply by issuing consistently timed motor commands. Rather, the neural system must integrate sensory information, system dynamic properties, and motor commands to link the state of one or more effectors to that of one or more other effectors [1,2]. For example, human patients who have lost all sensation (proprioception and touch) in their arm have trouble coordinating motion at different joints during reaching tasks [4], illustrating the need for the neural system to receive sensory input to maintain proper timing of muscle activity.

In its technical sense, higher coordination is not always advantageous. For example, although higher coordination between the left and right leg is desirable during normal walking, if one leg is encumbered by an obstacle, a momentary decrease in coordination (more independent motion of the left and right leg) allows the encumbered leg to free itself while the other leg maintains stride. Accordingly, different behaviors appear to require different levels of coordination [5-8]. For example, in humans, poor ball catching ability can be attributed to arm motions that are too coordinated [7] while poor arm reaching performance in stroke patients can be attributed to arm motions that are not sufficiently coordinated [5]. If human subjects are made to walk such that the left and right legs are on separate treadmills moving at different speeds, subjects change their patterns of interlimb coordination within minutes to restore a symmetric

gait pattern [6]. And coordination patterns vary among species in association with different behavioral and biomechanical requirements [8], consistent with reinforcement of particular coordination patterns through learning or natural selection.

What general principles, if any, determine the patterns of coordination during motion? One possibility is that coordination patterns are determined by speed. At faster speeds, animals have less time to perform neural computations and must increasingly rely on involuntary control; this shift in control may drive a shift in coordination patterns [9]. Consistent with this, changes in coordination variability have been observed for the same behavior at different speeds [10] and increasing the speed of motion is used in experiments to trigger a shift in coordination [11]. Another possibility is that the nature of the task determines patterns of coordination [2], specifically that motions of elements in a system are more coordinated when engaged in the same motor task. Consistent with this, coordination patterns among motions of the head, eyes, and hand [12] or between the left and right hands [13] in humans differ depending on the behavioral task. These two mechanisms are not mutually exclusive and coordination changes have been observed in motions of the jaw, neck, and forelimb of lizards at different speeds and when performing different tasks [8]. What is needed is a test of these two mechanisms on the same dataset: for a given motion sequence does task or speed best explain differences in coordination?

One group of organisms that face a particularly interesting coordination challenge is suction-feeding fishes. Fishes have more moving parts in their skulls (Fig. 1) than any other vertebrate—well over a dozen [14-16]. These movable elements are not all accessible to active and independent neural coordination: joints and ligaments connect these elements to form a multiloop linkage that passively couples the motion of certain elements [14-16]. Thus, suction-

feeding fishes use a combination of active actuation and passive coupling, effectively unfolding and collapsing the skeletal elements that surround the mouth to suck in fluid and prey items [17-20]. Suction feeding consists of at least two main phases, prey capture and intraoral transport (colloquially, 'swallowing'), and fish use distinct motion patterns for each phase [21-23]. However, whether these different motion patterns constitute distinct coordination patterns, indicating active coordination by the neural system, remains unknown.

As a part of a broader investigation into the biomechanics of suction feeding in fishes we measured the 3D, *in vivo* motion of seven bones in the skull and shoulder of channel catfish (*Ictalurus punctatus*) during the prey capture and transport phases of suction feeding. We initially chose channel catfish because their body form contrasts with a previously studied species, largemouth bass [24]. However, their cyclical feeding motions subsequently proved advantageous to measuring cross-correlation for the purpose of studying coordination. For motion measurements we used X-ray reconstruction of moving morphology (XROMM) [25] since the skeletal elements that function directly in expansion of the mouth are not all visible using surface motion capture approaches. Here we use this motion dataset to ask: does this motor system use distinct patterns of coordination and, if so, are these patterns best explained by differences in behavioral task (prey capture versus transport) or by differences in speed? Distinct patterns of coordination would be consistent with extensive active coordination and sensorimotor integration by the neural system in the skulls of fishes. And whether these patterns are best explained by task or speed would provide a clear test of competing hypotheses for the general determinants of coordination patterns in animal motion.

2. Materials and methods

(a) Animal care and surgical procedures

Channel catfish were obtained from Osage Catfisheries, Inc. (Osage Beach, MO, USA), housed individually at room temperature and regularly fed carnivore pellets. Animal care and procedures were approved by the Brown University Institutional Animal Care and Use Committee. Standard lengths (in cm) of Indiv1, Indiv2, and Indiv3 were 31.8, 30.5, and 37.5, respectively. After 1-2 months of training each fish to feed on demand, we performed surgery to implant tantalum spherical markers in 3 individuals for X-ray based motion tracking. We anesthetized the fish with buffered MS-222 (at 0.09-0.135 g/L) and administered an analgesic (0.4 mg/kg butorphanol). We unilaterally implanted 0.5 and 0.8 mm diameter markers into 8 skeletal elements (neurocranium, urohyal, and left-side post-temporal, cleithrum, suspensorium, operculum, lower jaw, and hyoid) and 0.8 mm diameter markers into the hypaxial muscles (intracranial motions in channel catfish appear to be bilaterally symmetric). Bone markers were implanted by pushing the bead into a hand-drilled hole having the same diameter as the bead. Muscle beads were injected through a hypodermic needle. We also implanted a polyethylene cannula through the rostral neurocranium to insert a pressure probe during experiments. Additional methodological details are provided in the supplementary material, including marker implantation sites (Figs. S1-3) and names (Tables S1-3).

(b) *In vivo* data collection

We recorded synchronous X-ray videos and intraoral pressures during suction feeding. Videos were recorded from two views (biplanar fluoroscopy) at 300 frames per second. For filming, individuals were given three different prey types: half or whole live earthworms, dead squid pieces, and carnivore pellets (Movies S1-2). In choosing prey types our main objective was to

elicit maximal changes in intraoral pressure for a related study quantifying suction power. We began experiments with Indiv1 and Indiv2 using a mix of prey types (Indiv1: 8 sinking pellets trials, 3 worm trials, and 4 squid trials; Indiv2: 5 sinking pellet trials, 9 worm trials, 1 squid trial). Then, after establishing that worms elicited the greatest intraoral pressure changes we filmed all Indiv3 trials (12 total) using only worms. Although worms elicited the greatest pressure differential, they did so only for some trials. Thus, even though all Indiv3 trials used worm prey, we obtained comparable pressure distributions for all three individuals (Table S4).

(c) XROMM animation

To convert marker motions into 3D rigid-body transformations for each skeletal element we used a workflow of marker tracking, reconstruction, and CT mesh unification known as XROMM animation. Marker X-ray trajectories were tracked using automation-assisted tracking tools in XMALab v1.3.9 [26]. A total of 36-38 beads were tracked (per individual) over a total of approximately 42,000 frames (all individuals). Hypaxial muscle strain was measured using fluoromicrometry, measuring the distance between the most rostral and the second or third most rostral hypaxial markers [27]. We performed camera calibration and marker reconstruction in XMALab. We segmented each skeletal element of interest from the CT scans and exported marker 3D coordinates in "CT space" using Horos v2.0.1 (horosproject.org). We performed all subsequent analyses using a new XROMM animation workflow (matools R package; github.com/aaronolsen) for R [28], including marker smoothing and aligning the smoothed 3D marker coordinates with the corresponding CT marker coordinates (unification; Movie S3) to animate each skeletal CT mesh. All mesh animations (e.g. Movie S3) were created using the

svgViewR R package [29]. The standard deviation in marker-to-marker distances within each skeletal element, one measure of precision, was 0.080 mm on average (Table S5).

(d) Joint model fitting

We used joint model fitting to reduce the full joint motion dataset (6 DoFs per skeletal element, 3 translational and 3 rotational, 36 total DoFs) to a smaller set of axes that represent the principal motions within the skull. We first trimmed out regions of each trial with little intracranial motion (e.g. swimming toward prey), leaving a total of 32,909 frames (Indiv1: 15,405 frames; Indiv2: 9,450; Indiv3: 8,054). We then fit models to the six joints connecting our skeletal elements of interest, fixing one element at each joint to characterize relative motion and concatenated all trials into a single sequence. To each joint we fit three models: a one-axis (hinge) joint, a two-axis (saddle) joint, and a three-axis (ball-and-socket) joint; here, the number of joint axes is also the number of DoFs. Model fitting was done using the 'fitMechanism' function in the linkR R package [30], which estimates a best-fitting center of rotation and axis or axes of rotation and the rotations about each axis. Specifically, the algorithm iteratively optimizes orientation and position of each axis, element pose, and rotations about each axis until the error or change in error drops below a specified threshold. Fit error was quantified using three landmarks distributed across each element. We then selected the lowest DoF model with an average maximum error less than 1% of head length (approx. 0.75 mm).

(e) Subsetting and binning data

To compare prey capture and intraoral transport we identified the capture and transport phase for each trial. The end of capture (and start of transport) was identified as the first time at which the

lower jaw fully elevated (closed) after the prey entered the mouth. We also divided each trial into open-close events for the purpose of comparing low- and high-speed motions (Indiv1: 61 events; Indiv2: 64; Indiv3: 45). An open-close event was defined as a single retraction and protraction of the pectoral girdle (each open-close event started and ended with the pectoral girdle in the retracted position). We used the minima of pectoral girdle retraction speed to delineate consecutive events because pectoral girdle retraction occurred consistently with mouth opening. We then binned these events evenly by individual into high and low speed bins based on the maximum pectoral girdle retraction speed during each event. The cut-offs separating low- and high-speed bins were set to obtain a similar number of open-close events in each bin and ranged from 48.5 to 66.4 deg/sec (Table S4). We repeated the same binning procedure based on the maximum intraoral pressure differential during each open-close event to test whether pressure has an effect on differences in cross-correlation. Results of the comparison based on pressure did not differ from those based on speed and so are not discussed further here but can be found in the supplementary material.

(f) Cross-correlation, motion integration and randomizations

From the joint model fitting we obtained a set of 8 significant rotations about each best-fit axis (concatenating all trials). We then measured the pairwise cross-correlation between each set of axis rotations ('motion pairs') for a total of 28 motion pairs. Cross-correlation takes as input two time-varying signals and returns the linear correlation coefficient between the two signals over a range of time lags (lags are added by shifting one signal relative to the other). For each pairwise combination we recorded the maximum cross-correlation across a lag range of -40 to 40 frames (-133 to 133 ms; lag.max=40 frames), so subsequent uses of 'cross-correlation' refer to this

maximum value (a re-analysis using a narrower lag range of -83 to 83 ms, lag.max=25 frames, did not affect the conclusions). Since cross-correlation implies just two signals we use 'motion integration' (or simply 'integration') to refer to the correlation between two or more motions [31]. This parallels the use of 'integration' in shape analysis to describe the correlation among multidimensional shape coordinates. We took the mean of all these pairwise cross-correlations as the total motion integration within the skull. We calculated cross-correlation using 'ccfDis' (matools R package), based on the standard cross-correlation function ('ccf') but modified for discontinuous time series. The 'ccfDis' function inserts buffers of NA values between concatenated sequences so that when one signal is slid relative to the other, the edge of one sequence does not overlap with the edge of a different sequence.

We assessed significance by resampling randomizations. The standard cross-correlation function does not return a significance statistic (high-frequency but independent oscillatory patterns can give relatively high, but non-significant, cross-correlation coefficients). Thus, to assess the significance of the cross-correlation coefficient we created a randomized sample by flipping (temporally reversing) one signal in each motion pair for each trial and calculating the cross-correlation, randomly choosing for each trial which of the two signals to flip. This process of flipping the signals creates a null distribution of motions for each pair that preserves the frequency and amplitude characteristics of the original data but removes temporal correspondence between the two signals. We calculated a *P*-value by dividing the number of iterations for which the randomized cross-correlation was greater or less than the actual cross-correlation (greater if the actual was positive, less if negative) by the number of randomized iterations. We formed a null distribution for assessing the significance of the cross-correlation difference between tasks (capture versus transport) by randomizing the designation of capture

versus transport within each trial. The significance of cross-correlation differences between bins (high versus low speed) was assessed in a similar way, randomizing the low and high bin designations by open-close event. Lastly, we assessed whether total integration differed significantly among individuals by randomizing the designation of individual across all 42 trials and calculating cross-correlations. All randomizations were repeated 999 times. We also tested for a difference in cross-correlation during capture versus transport by trial (i.e. calculating the mean cross-correlation for each behavior and trial and using a t-test to assess significance). Since this approach is more sensitive to spurious cross-correlations given the shorter sequences the lag range had to be reduced to -83 to 83 ms. However, the conclusions were the same as for the concatenated sequences and only the results from the concatenated sequences are presented here.

(g) Measuring coordination from motion integration

A challenge to measuring coordination is that although coordination produces correlated motion (i.e. motion integration), correlated motion is not produced solely by coordination [31]. We can think of three mechanisms that could cause correlated motion: extrinsic integrators, passive coupling, and active coordination. Extrinsic integrators include organism-environment interactions; for example, when trout swim in a flow with vortices, the vortices themselves drive much of the observed body undulations [32]. Passive coupling includes ligaments and other tissues that mechanically link elements. Motion integration not caused by extrinsic integrators or coupling results from active coordination by the neural system. For a fish feeding in still water, it is the skeletal elements that primarily drive fluid flow. Thus, observed motion patterns should result mostly from intrinsic mechanisms (coupling and coordination). Coupling, being structural, should generally be invariant across behaviors while coordination can vary motion integration

patterns for different behaviors (we note exceptions in the discussion). Thus, we infer that changes in motion integration patterns are caused by changes in coordination. Because we have used cross-correlation, our results may not be directly comparable to studies using continuous relative phase (CRP) or CRP variability [3]. CRP measures instantaneous correlation whereas cross-correlation measures correlation over a given time range. Due to sample size limitations we cannot measure cross-correlation variability in a manner analogous to CRP variability. We used cross-correlation because, unlike CRP, it can incorporate lags. Lastly, although 'coordination' is often used in the literature to refer to what we call 'integration', we use 'coordination' to refer solely to the active component of motion integration.

3. Results

(a) Behavior

For most trials we observed channel catfish perform a complete feeding sequence, starting with search for the prey and ending with transport of the prey into the esophagus (Fig. 2; Movies S4-5). Throughout the entire sequence (Fig. 2a-h), we observed repeated opening and closing of the mouth. During prey search, the fish whisked its barbels back and forth while rummaging along the bottom of the tank with its head (Fig. 2a-c). Only after a barbel made physical contact with the prey did the fish suck the prey into its mouth (Fig. 2c-d); fish did not appear to make any use of visual cues. After engulfing the prey, the fish retreated by swimming backward while simultaneously beginning intraoral transport of the prey (Fig. 2e-h). We used the first mouth closure immediately after the prey entered the mouth (Fig. 2e) to divide each feeding sequence into prey capture (Fig. 2a-d) and intraoral transport (Fig. 2e-h).

(b) Intracranial motion

We observed substantial motion (rotations about a primary axis of at least 15 degrees) at five of the six joints of interest in this study during both capture and transport (Fig. 3; Figs. S4-9; Movie S3). The exception was the neurocranium-post-temporal joint, where rotations were generally less than 4 degrees (Figs. S4-6) and were not correlated with any other intracranial motions (Figs. S10-12); for this reason we excluded motion at the post-temporal joint from subsequent analyses. Based on the magnitude of rotations about each axis and mean maximum model fit errors we found that one rotational axis (a hinge model) was sufficient to describe motions of the suspensorium and pectoral girdle (Fig. 3a-b). For the suspensorium, secondary and tertiary rotations were less than 2 degrees (Figs. S4e-3e) and one-axis model errors were less than 1% head length for all individuals (Figs. S4f-3f). For the pectoral girdle, secondary and tertiary rotations were less than 3 degrees (Figs. S4h-3h) and one-axis model errors only significantly exceeded 1% head length for Indiv3 (Fig. S6i).

We found that two rotational axes (a saddle joint model) were needed to describe the motions of the operculum, lower jaw, and hyoid, all relative to the suspensorium (Fig. 6c-e). For the operculum, two-axis model errors were less than 1% head length for all individuals (Figs. S4l-6l). For the lower jaw, two-axis model errors significantly exceeded 1% head length for Indiv1 (Fig. S4o). For the hyoid two-axis model errors significantly exceeded 1% head length for Indiv2 and Indiv3 (Figs. S5r and S6r, respectively). However, tertiary rotations (oriented approximately along the long axis of the hyoid) may be unreliable given our inability to implant markers far from the long axis of the hyoid. Thus, we used only the first two axes. Motion names for each joint (e.g. suspensorium abduction; see Fig. 3) refer to positive rotations about the

278 corresponding axis (Fig. 3a-e), following the right-hand rule. The rotations about these eight axes
279 represent the principal motions within the skull (Fig. 3f; results for all individuals in Figs. S7-9).
280
281 **(c) Motion integration patterns and coordination changes**
282 Intracranial motions in channel catfish were highly and significantly cross-correlated throughout
283 feeding (Fig. 4a-b, upper diagonal; results for all individuals in Figs. S13-15). Of the 28 pairwise
284 motion comparisons, rotations between at least 27 pairs were significantly cross-correlated
285 during capture ($P < 0.05$; Fig. 4a) and rotations between at least 23 pairs were significantly
286 cross-correlated during transport (Fig. 4b) for all individuals. Two motion pairs showed
287 particularly high cross-correlations (Fig. 4a-b, upper right triangle) and 0 ms lags (Fig. 4a-b,
288 lower left triangle): pectoral girdle retraction and hyoid retraction (Fig. 4d) and opercular
289 elevation and lower jaw depression. Among the motion pairs with the lowest cross-correlation
290 was pectoral girdle retraction and lower jaw ventral roll (Fig. 4e). In spite of significant
291 intracranial motion integration during prey capture and transport, we detected several significant
292 decreases in integration from capture to transport (Fig. 4c). Of all significant changes during
293 capture versus transport, at least 75% were decreases: 14 of 14 for Indiv1, 13 of 17 for Indiv2
294 (Fig. 4c), and 12 of 15 for Indiv3. One motion pair for which this decrease was particularly
295 pronounced was pectoral girdle retraction and opercular dilation (Fig. 4f).
296 A decrease was also observed in the mean of all pairwise cross-correlations (total
297 intracranial integration): integration dropped significantly by 0.11-0.16 (20-29%) from capture to
298 transport for all individuals ($P < 0.01$; Fig. 5a-b). In contrast, no significant differences in total
299 integration were detected between mouth open-close events grouped by high versus low pectoral
300 girdle retraction speed (Fig. 5a-b). Some differences among individuals were detected in mean

integration (Fig. 5a-b, carets), however no significant individual differences were detected in the motion integration change from capture to transport (Fig. 5b; $P < 0.05$). Thus, although individuals showed slight differences in overall intracranial integration, decreases in integration from capture to transport were consistent for all individuals. The decrease in integration from prey capture to transport in channel catfish affected all five cranial skeletal elements of interest in this study (Fig. 6; Table S6). Each cranial element showed a decrease in cross-correlation strength with at least two other elements by a magnitude greater than the mean decrease across all pairwise comparisons (0.14). Pectoral girdle retraction was the motion most strongly cross-correlated with all other motions. Pectoral girdle retraction was also significantly correlated with shortening of the hypaxial muscles (Fig. 6), with no significant change between capture and transport ($P < 0.05$). In contrast, suspensorium and operculum motions were among the most variable in their cross-correlation with other elements.

4. Discussion

In this study we used a dataset of motions throughout the skull of channel catfish to uncover a significant shift in patterns of motion integration (correlations among two or more motion sequences) during feeding. We argue that this shift in integration is due primarily to changes in coordination by the neural system. We find that this shift in integration is not explained by speed but rather by behavioral objective (prey capture versus transport), supporting the hypothesis that it is the nature of a task that determines coordination patterns. Specifically, we find that intracranial motions are more coordinated during prey capture than during prey transport. Our finding that shifts in coordination affect all five cranial skeletal elements suggests that the fish cranial linkage, in spite of multiple couplings, has greater degrees of freedom (DoFs) of motion

than generally recognized. And our finding that tightly integrated motions during prey capture are mediated by coordination suggests an important role for sensory feedback in motor control of the fish skull.

Despite only collecting motion data we can still conclude that most of the motion integration changes that we have observed are due to coordination. Ruling out extrinsic causes of motion integration, we are left with intrinsic mechanisms: passive coupling and active coordination (see Methods section 2g). Although correlated motion due to coupling should generally be invariant across behaviors (because such couplings are always present), we can think of two ways in which coupling could cause varying motion integration patterns, referred to here as variable passive coupling (VPC). The first is viscoelasticity of coupling elements such as connective tissues. Because of viscoelasticity, a coupling element could provide tighter coupling the faster it is pulled, creating a difference in integration when the system is actuated at different speeds. However, we observed no significant difference in total integration between high- and low-speed motions (Fig. 5). We would especially expect viscoelastic VPC at direct ligamentous couplings, such as between lower jaw depression and opercular elevation, coupled by the interoperculomandibular ligament. However, the cross-correlation between these motions changes less than 0.03 for low- versus high-speed events (Figs. S13f-15f). The short length of the ligaments relative to the size of the bones in channel catfish skulls may explain why any length changes in connective tissues has little effect in varying integration patterns.

A second potential VPC mechanism is non-linear motion transmission between two links in a linkage. For example, in a 1-DoF four-bar linkage input link motion relative to output link motion is often non-linear. If such a four-bar is actuated over a consistent range between two behaviors then the input-output cross-correlation will be consistent. However, if actuated over

different ranges, one effectively "samples" different regions of this non-linear relationship, resulting in variable input-output cross-correlations. Importantly, the linkage must have one degree of freedom so that motion of one link follows directly from the motion of another. None of the skeletal elements investigated here appear to be coupled by 1-DoF linkages. We recently showed that the lower jaw-operculum linkage in largemouth bass functions as a 3-DoF 3D four-bar [16] and this linkage appears to have at least as much mobility in channel catfish. Similarly, the pectoral-hyoid linkage [14] forms a six-bar linkage in three dimensions, which should have at least 2 DoFs. Furthermore, four of the six skeletal element pairs that show the greatest change in integration (Fig. 6) are not even directly coupled by a linkage.

Not only can we rule out passive mechanisms as a principal cause of the observed changes in integration, but we can also identify active mechanisms that can fully account for these changes. At least 10 different muscles (8 intracranial and 2 axial muscle groups) attach to the skeletal elements of interest here (Fig. 6), with at least two muscles attached to each element. Studies of cranial muscle activity in other species of fishes have found that these muscles are active during feeding [21,23,33], and that their activation patterns can differ significantly between prey capture and other feeding behaviors [21,23,33]. Muscle architecture and general patterns of muscle activation across fishes are fully and uniquely congruent with active neural control as the modifier of motion integration patterns between prey capture and transport. For this reason we conclude that the shift in integration observed here is primarily a shift in coordination.

Our results suggest that sensorimotor integration maintains the effective timing of intracranial motions within the fish skull [34]. Although the fish skull is frequently modeled as a series of 2D, 1-DoF four-bar linkages [e.g. 14,15] it is also recognized that fish are capable of

moving the bones within their heads in multiple, independent ways [33,35]. Based on our results, the channel catfish skull likely has at least 5 DoFs: we observe significant changes in coordination among five main skeletal elements (Fig. 6) and the opercular linkage and pectoral-hyoid linkages (which, as mentioned previously, likely have 3 and 2 DoFs, respectively) can account for at least 5 DoFs. Each DoF in a system represents an independent dimension along which position and motion must be controlled. Thus, with greater DoFs comes a need for greater active control and coordination, which in turn requires sensory feedback to maintain the relative timings among moving parts [1,2]. Evidence for sensory feedback in the fish skull has been reported previously, particularly the ability of fish to modulate their feeding kinematics in response to prey type and position [33-35]. Our findings confirm the role of sensory feedback in modulating kinematics and suggest an additional role in coordinating the relative timing of intracranial motions.

Why are intracranial motions in channel catfish more coordinated during capture than during transport? In suction-feeding fishes intracranial motions function to direct fluid flow. During capture these motions follow a stereotyped and evolutionarily conserved anterior-to-posterior sequence: lower jaw depression, hyoid retraction, and opercular dilation [17,36]. This sequence creates a single, unidirectional flow into the mouth [18,20]. The relative timing of these events is key to performance. Opercular dilation, which allows caudal outflow, enables fish to ingest more water than can be accommodated by the oral cavity [18]. And wave-like, rather than simultaneous, expansion prolongs fluid flow so that maximum fluid speed better coincides with peak gape [18,37]. As expected, during capture in channel catfish we find an anterior-to-posterior wave starting with lower jaw depression at 0 ms, suspensorial abduction at 30 ms, hyoid retraction at 36 ms, and opercular dilation at 76 ms. However, during transport this

sequence breaks down: lags become more variable, opercular dilation generally decouples from hyoid retraction, and cross-correlations decrease. This attenuation of the anterior-to-posterior wave during transport shows that the wave is not built into the mechanical linkages of the skull [37], but rather results from active, neural control. Much of the decrease in coordination that we observe from capture to transport may be due to a shift away from the stereotyped anterior-to-posterior wave and toward a more variable or modular pattern of timings.

Motions may be less cross-correlated during transport simply because timings during that phase are not as crucial to performance. A relaxation of timing constraints would free the system from adhering to a single coordination program, increasing variability and decreasing cross-correlations. Additionally, it is possible that alternative ways of partitioning this motion dataset would reveal alternative coordination patterns. For example, “transport” may contain multiple discrete coordination patterns, which when grouped together appear as lower coordination. A final explanation relates back to the general question of what determines coordination patterns in motor systems. One hypothesis is that the motions of elements in a system are more coordinated when they are engaged in the same motor task [2]. In the case of fish feeding the “number of flows” generated by the skull may represent the number of tasks. High coordination during prey capture can then be explained as all of the cranial elements engaged in a single task (a single flow throughout the mouth), whereas lower coordination during transport reflects the cranial elements engaging in multiple tasks, independently accelerating fluid at one or more localized regions within the mouth to reposition and move prey. Future work investigating how intracranial motions relate to intraoral fluid flows and prey transport performance will ultimately resolve these questions and increase our understanding of why particular motor tasks are accomplished by different coordination patterns.

Competing interests. We have no competing interests.

Author contributions. Designed data collection: A.M.O., L.P.H., A.L.C., E.L.B. Performed data collection: A.M.O., L.P.H. Analyzed data: A.M.O. Conceived this study and wrote the paper: A.M.O. Provided comments on paper: A.L.C., E.L.B., L.P.H.

Data deposition. We deposited data for this publication in the XMAPortal (xmaportal.org) in the study 'Catfish Suction Feeding' (permanent ID BROWN61), in accordance with best practices for video data management [38]. Processed kinematic data (.csv format) are published with this study as a supplemental dataset. All custom R code referenced here can be found at github.com/aaronolsen.

Acknowledgments. We thank Tara Bozzini, Mariah Nuzzo, Shahn Thaliffdeen, Connor Johnson, and Alejandro Romero for assistance with marker tracking, Erika Tavares and Yordano Jiménez for assistance with data collection, Kenny Breuer, Nicolai Konow, Peter Falkingham, and Jeff Moore for helpful discussion, and three anonymous reviewers for critical feedback that greatly improved the manuscript.

Funding. This research was funded by National Science Foundation grants 1612230 to A.M.O., 1655756 to E.L.B. and A.L.C., 1661129 to E.L.B, and the Bushnell Research and Education Fund.

References

1. Todorov E, Jordan MI. 2002 Optimal feedback control as a theory of motor coordination. *Nat. Neurosci.* **5**, 1226–1235. (doi:10.1038/nn963)
2. Diedrichsen J, Shadmehr R, Ivry RB. 2010 The coordination of movement: optimal feedback control and beyond. *Trends Cogn. Sci.* **14**, 31–39. (doi:10.1016/j.tics.2009.11.004)
3. Wheat JS, Glazier PS. 2005 Measuring coordination and variability in coordination. In *Human kinetics* (eds K Davids, S Bennett & K Newell), pp. 167–181. Sheridan Books.
4. Forget R, Lamarre Y. 1987 Rapid elbow flexion in the absence of proprioceptive and cutaneous feedback. *Hum. Neurobiol.* **6**, 27–37.
5. Cirstea MC, Mitnitski AB, Feldman AG, Levin MF. 2003 Interjoint coordination dynamics during reaching in stroke. *Exp. Brain Res.* **151**, 289–300. (doi:10.1007/s00221-003-1438-0)
6. Reisman DS, Block HJ, Bastian AJ. 2005 Interlimb coordination during locomotion: what can be adapted and stored? *J. Neurophysiol.* **94**, 2403–2415. (doi:10.1152/jn.00089.2005)
7. Utley A, Steenbergen B, Astill SL. 2007 Ball catching in children with developmental coordination disorder: control of degrees of freedom. *Dev. Med. Child Neurol.* **49**, 34–38. (doi:10.1017/S0012162207000096.x)
8. Montuelle SJ, Herrel A, Libourel P, Daillie S, Bels VL. 2012 Flexibility in locomotor-feeding integration during prey capture in varanid lizards: effects of prey size and velocity. *J. Exp. Biol.* **215**, 3823–3835. (doi:10.1242/jeb.072074)
9. Biewener AA, Daley MA. 2007 Unsteady locomotion: integrating muscle function with whole body dynamics and neuromuscular control. *J. Exp. Biol.* **210**, 2949–2960. (doi:10.1242/jeb.005801)

10. Cazzola D, Pavei G, Preatoni E. 2016 Can coordination variability identify performance factors and skill level in competitive sport? The case of race walking. *J. Sport Health Sci.* **5**, 35–43. (doi:10.1016/j.jshs.2015.11.005)
11. Mechsner F, Kerzel D, Knoblich G, Prinz W. 2001 Perceptual basis of bimanual coordination. *Nature (Lond.)***414**, 69. (doi:10.1038/35102060)
12. Pelz J, Hayhoe M, Loeber R. 2001 The coordination of eye, head, and hand movements in a natural task. *Exp. Brain Res.* **139**, 266–277. (doi:10.1007/s002210100745)
13. Diedrichsen J. 2007 Optimal task-dependent changes of bimanual feedback control and adaptation. *Curr. Biol.***17**, 1675–1679. (doi:10.1016/j.cub.2007.08.051)
14. Westneat MW. 1990 Feeding mechanics of teleost fishes (Labridae; Perciformes): A test of four-bar linkage models. *J. Morphol.* **205**, 269–295. (doi:10.1002/jmor.1052050304)
15. Van Wassenbergh S, Herrel A, Adriaens D, Aerts P. 2005 A test of mouth-opening and hyoid-depression mechanisms during prey capture in a catfish using high-speed cineradiography. *J. Exp. Biol.* **208**, 4627–4639. (doi:10.1242/jeb.01919)
16. Olsen AM, Camp AL, Brainerd EL. 2017 The opercular mouth-opening mechanism of largemouth bass functions as a 3D four-bar linkage with three degrees of freedom. *J. Exp. Biol.* **220**, 4612–4623. (doi:10.1242/jeb.159079)
17. Ferry-Graham LA, Lauder GV. 2001 Aquatic prey capture in ray-finned fishes: a century of progress and new directions. *J. Morphol.* **248**, 99–119. (doi:10.1002/jmor.1023)
18. Day SW, Higham TE, Cheer AY, Wainwright PC. 2005 Spatial and temporal patterns of water flow generated by suction-feeding bluegill sunfish *Lepomis macrochirus* resolved by particle image velocimetry. *J. Exp. Biol.* **208**, 2661–2671. (doi:10.1242/jeb.01708)

19. Van Wassenbergh S, Aerts P, Herrel A. 2006 Hydrodynamic modelling of aquatic suction performance and intra-oral pressures: limitations for comparative studies. *J. Royal Soc. Interface* **3**, 507–514. (doi:10.1098/rsif.2005.0110)
20. Van Wassenbergh S, Aerts P. 2009 Aquatic suction feeding dynamics: insights from computational modelling. *J. Royal Soc. Interface* **6**, 149–158. (doi:10.1098/rsif.2008.0311)
21. Turingan RG, Wainwright PC. 1993 Morphological and functional bases of durophagy in the queen triggerfish, *Balistes vetula* (Pisces, Tetraodontiformes). *J. Morphol.* **215**, 101–118. (doi:10.1002/jmor.1052150202)
22. Gillis G, Lauder G. 1995 Kinematics of feeding in bluegill sunfish: is there a general distinction between aquatic capture and transport behaviors? *J. Exp. Biol.* **198**, 709–720.
23. Alfaro ME, Janovetz J, Westneat MW. 2001 Motor control across trophic strategies: muscle activity of biting and suction feeding fishes. *Am. Zool.* **41**, 1266–1279. (doi:10.1093/icb/41.6.1266)
24. Camp AL, Roberts TJ, Brainerd EL. 2015 Swimming muscles power suction feeding in largemouth bass. *Proc. Natl. Acad. Sci.* **112**, 8690–8695. (doi:10.1073/pnas.1508055112)
25. Brainerd EL, Baier DB, Gatesy SM, Hedrick TL, Metzger KA, Gilbert SL, Crisco JJ. 2010 X-ray reconstruction of moving morphology (XROMM): precision, accuracy and applications in comparative biomechanics research. *J. Exp. Zool. Part A.* **313**, 262–279. (doi:10.1002/jez.589)
26. Knörlein BJ, Baier DB, Gatesy SM, Laurence-Chasen JD, Brainerd EL. 2016 Validation of XMALab software for marker-based XROMM. *J. Exp. Biol.* **219**, 3701–3711. (doi:10.1242/jeb.145383)

27. Camp AL, Astley HC, Horner AM, Roberts TJ, Brainerd EL. 2016 Fluoromicrometry: a method for measuring muscle length dynamics with biplanar videofluoroscopy. *J. Exp. Zool. Part A.* **325**, 399–408. (doi:10.1002/jez.2031)
28. R Core Team R. 2018 *R: A Language and Environment for Statistical Computing*. URL www.R-project.org/.
29. Olsen AM. 2018 svgViewR: 3D Animated Interactive Visualizations using SVG. URL cran.r-project.org/package=svgViewR.
30. Olsen AM, Westneat MW. 2016 Linkage mechanisms in the vertebrate skull: Structure and function of three-dimensional, parallel transmission systems. *J. Morphol.* **277**, 1570–1583. (doi:10.1002/jmor.20596)
31. Wainwright PC, Mehta RS, Higham TE. 2008 Stereotypy, flexibility and coordination: key concepts in behavioral functional morphology. *J. Exp. Biol.* **211**, 3523–3528. (doi:10.1242/jeb.007187)
32. Liao JC, Beal DN, Lauder GV, Triantafyllou MS. 2003 Fish exploiting vortices decrease muscle activity. *Science (Wash. D.C.)* **302**, 1566–1569. (doi:10.1126/science.1088295)
33. Konow N, Camp AL, Sanford CPJ. 2008 Congruence between muscle activity and kinematics in a convergently derived prey-processing behavior. *Integr. Comp. Biol.* **48**, 246–260. (doi:10.1093/icb/icn045)
34. Aerts P. 1990 Variability of the fast suction feeding process in *Astatotilapia elegans* (Teleostei: Cichlidae): a hypothesis of peripheral feedback control. *J. Zool. (Lond.)* **220**, 653–678. (doi:10.1111/j.1469-7998.1990.tb04741.x)

526 35. Gardiner JM, Atema J, Hueter RE, Motta PJ. 2017 Modulation of shark prey capture
527 kinematics in response to sensory deprivation. *Zoology (Jena)* **120**, 42–52.
528 (doi:10.1016/j.zool.2016.08.005)
529 36. Gibb AC, Ferry-Graham L. 2005 Cranial movements during suction feeding in teleost fishes:
530 are they modified to enhance suction production? *Zoology (Jena)* **108**, 141–153.
531 (doi:10.1016/j.zool.2005.03.004)
532 37. Bishop KL, Wainwright PC, Holzman R. 2008 Anterior-to-posterior wave of buccal
533 expansion in suction feeding fishes is critical for optimizing fluid flow velocity profile. *J.*
534 *Royal Soc. Interface* **5**, 1309–1316. (doi:10.1098/rsif.2008.0017)
535 38. Brainerd EL, Blob RW, Hedrick TL, Creamer AT, Müller UK. 2017 Data management
536 rubric for video data in organismal biology. *Integr. Comp. Biol.* **57**, 33–47.
537 (doi:10.1093/icb/icx060)

538 **Figure 1.** Mobile skeletal elements of the channel catfish skull (latero-frontal view). The '+'
539 symbol indicates ossifications included within the skeletal element names used in the text.
540 Abbreviations: Left (L), insertion (ins), origin (ori).
541
542 **Figure 2.** Channel catfish feeding behavior. For this study we separated feeding into two tasks or
543 phases: prey capture (a-d) and prey intraoral transport (e-h). Timing of events (lower right
544 corner) is variable; only approximate timings are shown.
545
546 **Figure 3.** Rotations at the principal intracranial joints in channel catfish during feeding for
547 Indiv2. Colored arrows in (a-e) are best-fit motion axes with corresponding rotations in degrees
548 (f) about each axis across all trials from this individual. Only axes with significant rotations are
549 shown. The mobile body in each pair is shown in the most extreme poses over its range of
550 motion. For the two-axis joint model, the secondary axis moves with the mobile body and is
551 therefore shown in multiple poses. In (f), inverted black triangles indicate the start of each trial
552 (N = 15 trials). The capture and transport phases were identified for each feeding trial. The
553 purple and orange bars indicate the duration of the capture (purple) and transport (orange) phases
554 for each trial. See Figs. S7-S9 for corresponding figures for all individuals.
555
556 **Figure 4.** Cranial motion integration patterns in channel catfish during feeding for Indiv2.
557 Squares in (a-c) represent pairwise comparisons of intracranial motions, with cross-correlations
558 in the upper right and lag times in the lower left. Positive lag times indicate that the left row label
559 motion precedes the top column label motion; for example, during capture, lower jaw depression
560 precedes pectoral girdle retraction by 47 ms. Negative lag times indicates that the left label

follows the top column label. Because motions are generally more integrated during capture (a) than during transport (b), changes in absolute cross-correlation are mostly negative (c). Asterisks indicate significant cross-correlations in (a-b) and significant shifts in cross-correlation in (c), based on randomization tests. Three examples of motion cross-correlation relationships are shown in (d-f). See Figs. S13-S15 for corresponding figures for all individuals.

Figure 5. Mean motion integration differences by task and speed for all individuals. Mean intracranial motion integration was significantly greater ($P < 0.01$, asterisks) during capture than during transport for all individuals (a-b, left). In contrast, no significant differences in mean integration were found between mouth open-close events grouped by speed (a-b, right). One significant individual difference was identified ($P < 0.05$, carets) but not in the mean integration differences during capture versus transport (b, left). Values within bars are mean (SD) in (a) and mean in (b). Significance was determined by randomization tests.

Figure 6. Summary of coordination changes in the channel catfish skull during feeding. Nodes represent each skeletal element and edges represent the mean motion integration between skeletal elements (mean of all cross-correlations including that element for all individuals). Black edges indicate where integration changes from capture to transport by less than 0.14 (the mean difference for all pairwise comparisons); purple and orange edges indicate integration changes greater than 0.14. Edge thickness is proportional to the associated integration value. See the corresponding Table S6 for results by individual.

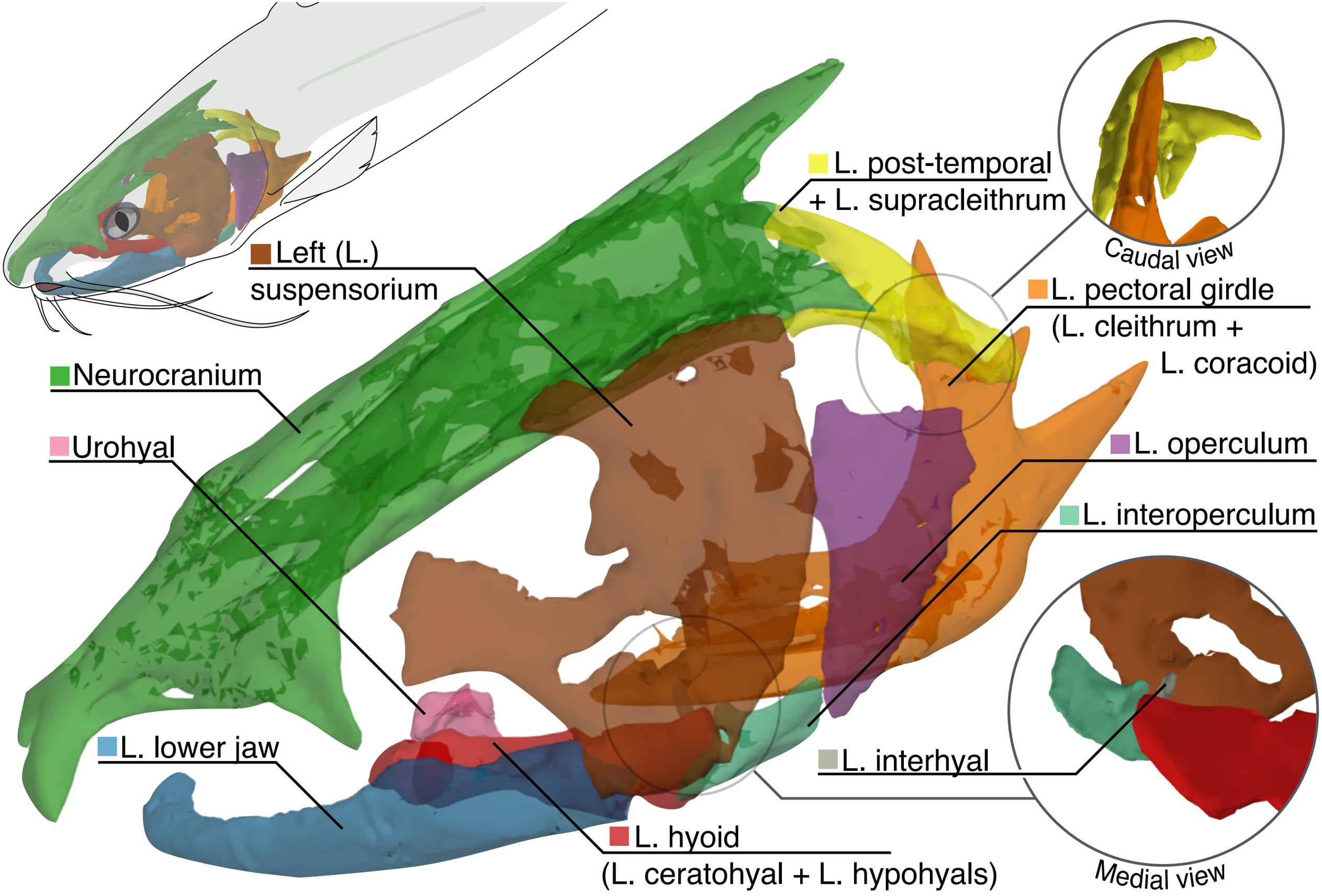
Left (L.)
suspensorium
Neurocranium
Urohyal
L. lower jaw
L. post-temporal
+ L. supracleithrum
Caudal view
L. pectoral girdle
(L. cleithrum +
L. coracoid)
L. operculum
L. interoperculum
L. interhyal
L. hyoid
(L. ceratohyal + L. hypohyals)
Medial view

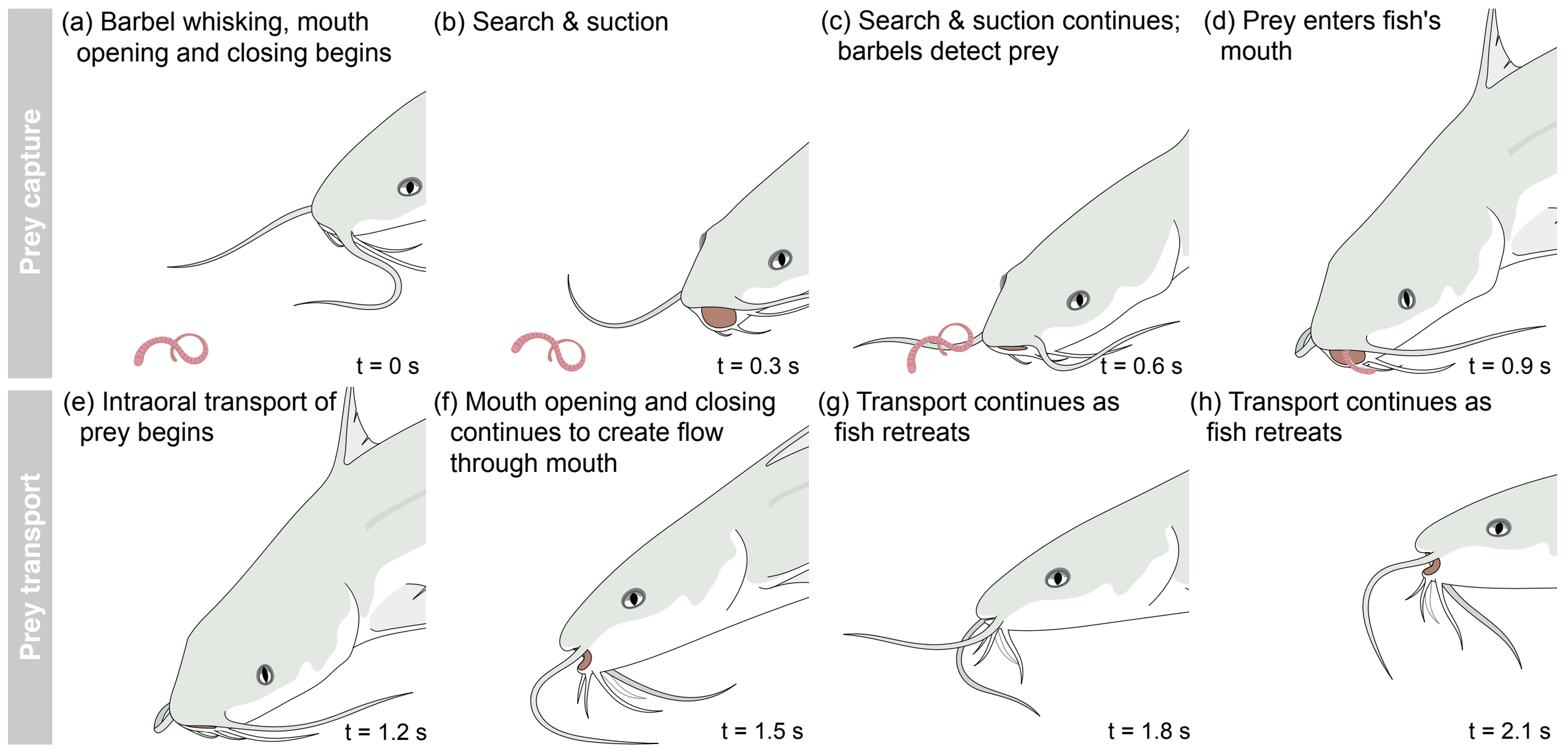
Prey capture
(a) Barbel whisking, mouth opening and closing begins
t = 0 s
(b) Search & suction
t = 0.3 s
(c) Search & suction continues; barbels detect prey
t = 0.6 s
(d) Prey enters fish's mouth
t = 0.9 s
Prey transport
(e) Intraoral transport of prey begins
t = 1.2 s
(f) Mouth opening and closing continues to create flow through mouth
t = 1.5 s
(g) Transport continues as fish retreats
t = 1.8 s
(h) Transport continues as fish retreats
t = 2.1 s

(a) Suspensorium

ABDUCTION

(b) Pectoral girdle

RETRACTION

(c) Operculum

DILATION
ELEVATION

(d) Lower jaw

DEPRESSION
VENTRAL ROLL

(e) Hyoid

RETRACTION
DEPRESSION

(f) Intracranial rotations

Prey capture

Intraoral transport

T01 T02 T03 T04 T05 T06 T07 T08 T09 T10 T11 T12 T13 T14 T1

SU ABD

PG RETR

OP DIL

OP ELEV

LJ DEPR

LJ VROL

HY RETR

HY DEPR

Rotations (deg)

20 deg

0 1 2 3 4 5 6 7 8 9 10 11 12 13 14 15 16 17 18 19 20 21 22 23 24 25 26 27 28 29 30 31

Time (sec)

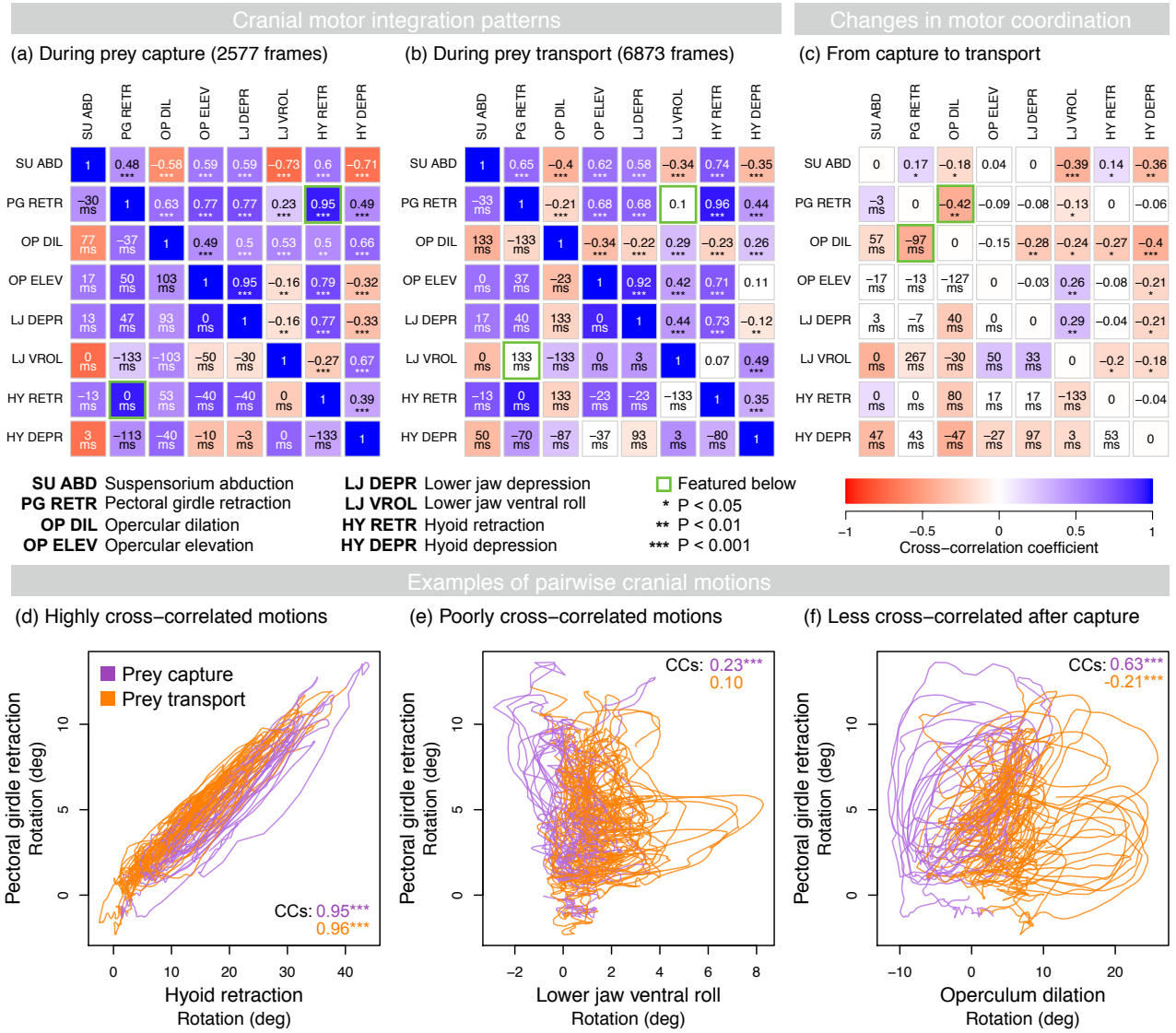
Cranial motor integration patterns
Changes in motor coordination
(a) During prey capture (2577 frames)
(b) During prey transport (6873 frames)
(c) From capture to transport
SU ABD
PG RETR
OP DIL
OP ELEV
LJ DEPR
LJ VROL
HY RETR
HY DEPR
SU ABD Suspensorium abduction
PG RETR Pectoral girdle retraction
OP DIL Opercular dilation
OP ELEV Opercular elevation
LJ DEPR Lower jaw depression
LJ VROL Lower jaw ventral roll
HY RETR Hyoid retraction
HY DEPR Hyoid depression
Featured below
* P < 0.05
** P < 0.01
*** P < 0.001
−1
−0.5
0
0.5
1
Cross−correlation coefficient
Examples of pairwise cranial motions
(d) Highly cross−correlated motions
(e) Poorly cross−correlated motions
(f) Less cross−correlated after capture
Prey capture
Prey transport
CCs: 0.95*** 0.96***
CCs: 0.23*** 0.10
CCs: 0.63*** -0.21***
Pectoral girdle retraction Rotation (deg)
Hyoid retraction Rotation (deg)
Lower jaw ventral roll Rotation (deg)
Operculum dilation Rotation (deg)

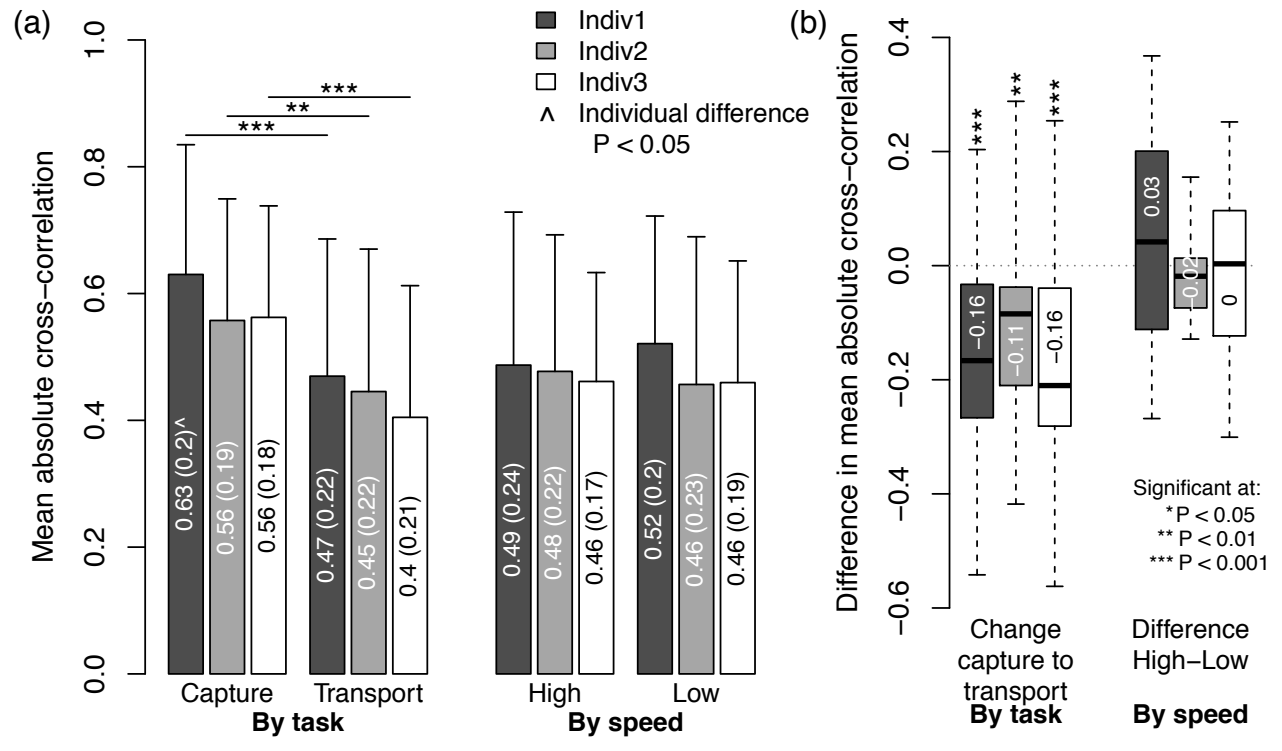
(a)
Mean absolute cross−correlation
0.0
0.2
0.4
0.6
0.8
1.0
Indiv1
Indiv2
Indiv3
^ Individual difference
P < 0.05
***
**
***
0.63 (0.2)^
0.56 (0.19)
0.56 (0.18)
0.47 (0.22)
0.45 (0.22)
0.4 (0.21)
0.49 (0.24)
0.48 (0.22)
0.46 (0.17)
0.52 (0.2)
0.46 (0.23)
0.46 (0.19)
Capture
Transport
By task
High
Low
By speed
(b)
Difference in mean absolute cross−correlation
−0.6
−0.4
−0.2
0.0
0.2
0.4
***
**
***
−0.16
−0.11
−0.16
0.03
−0.02
0
Change capture to transport
By task
Difference High−Low
By speed
Significant at:
*P < 0.05
** P < 0.01
*** P < 0.001

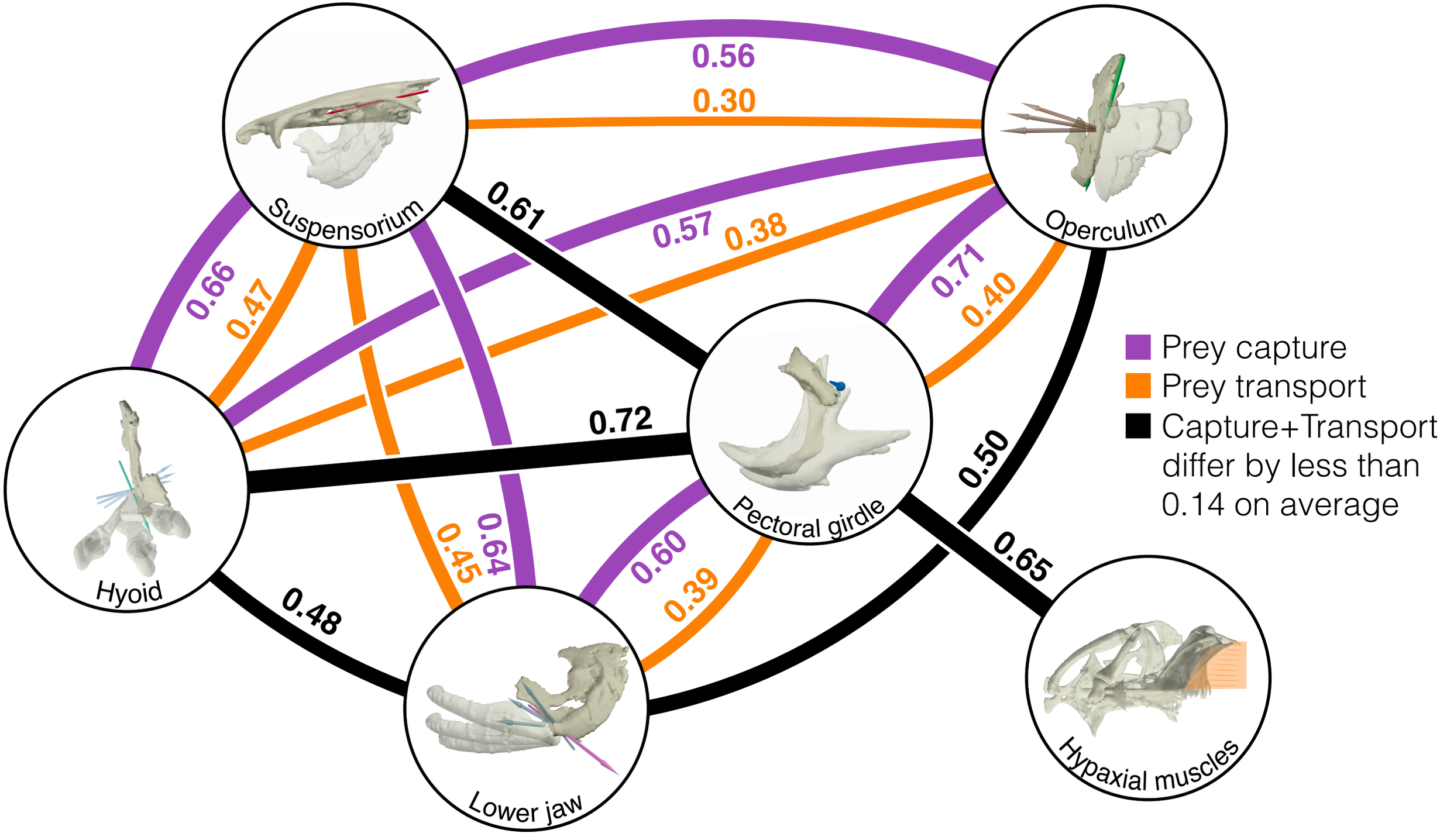
Suspensorium
Operculum
Hyoid
Pectoral girdle
Lower jaw
Hypaxial muscles
0.56
0.30
0.61
0.57
0.38
0.66
0.47
0.71
0.40
0.72
0.50
0.64
0.45
0.60
0.39
0.48
0.65
Prey capture
Prey transport
Capture+Transport differ by less than 0.14 on average